KLOE MEMO n^{o}195

August 13, 1999

Measurement of the hadronic cross section $\sigma(e^+e^- \to \pi^+\pi^-)$ from initial state radiative events $\pi^+\pi^-\gamma$ with the KLOE detector

Gabriella Cataldi, Achim Denig, Wolfgang Kluge, Graziano Venanzoni

Institut für Experimentelle Kernphysik, Universität Karlsruhe

Abstract

Several proposals have been made to use the photon emitted in the initial state in $e^+e^- \to \pi^+\pi^-\gamma$ events in order to scan the hadronic cross section $\sigma(e^+e^- \to \pi^+\pi^-)$ with the energy of the photon. This memo explores this possibility for the KLOE detector. By means of extensive Monte Carlo studies it is shown how it is possible to achieve an accuracy of the order of 1% for the selection and identification of these events for each interval of the center of mass energy of the two pions. This accuracy is mandatory in order to perform precision measurements of a_μ and $\alpha(M_Z^2)$. Statistics, systematics, resolution effects and background rejection are discussed.

1 Introduction

One of the topics to be pursued with DAΦNE concerns the measurement of hadronic cross section $\sigma(e^+e^- \to hadrons)$ [1]. Such a measurement, if performed at the 1% accuracy level, offers significant tests of the Standard Model *via* a very precise measurement of the anomalous magnetic moment a_μ and the effective fine structure constant at the Z-peak $\alpha(M_Z^2)$ [2].

Both the theoretical errors on a_μ and $\alpha(M_Z^2)$ are dominated by the uncertainties of the contribution of the light quarks to the photon vacuum polarization [2]. At low energies, where the perturbative QCD cannot be applied, the measurement of $\sigma(e^+e^- \to hadrons)$ turns out to be very useful, since it allows to evaluate the hadronic contribution to the photon vacuum polarization by using dispersion relations, as follows [2, 3]:

$$\Pi'_\gamma(q^2) - \Pi'_\gamma(0) = \frac{q^2}{\pi}\int_0^\infty ds \frac{Im\Pi'_\gamma(s)}{s(s-q^2-i\epsilon)} = \frac{q^2}{12\pi^2}\int_0^\infty ds \frac{R(s)}{s(s-q^2-i\epsilon)}$$

where $\Pi_\gamma(q^2) = s\Pi'_\gamma(q^2)$ is the photon self energy and $R(s)$ is equal to $\frac{\sigma(e^+e^-\rightarrow hadrons)}{\frac{4\pi\alpha^2(s)}{3s}}$. The hadronic contribution to a_μ and $\Delta\alpha(M_Z^2)$ [1] can be therefore written as:

$$a_\mu^{had} = (\frac{\alpha m_\mu}{3\pi})^2 \int_{4m_\pi^2}^\infty ds \frac{R(s)\hat{K}(s)}{s^2} \quad (1)$$

$$\Delta\alpha^{had}(M_Z^2) = -\frac{\alpha m_Z^2}{3\pi}\mathrm{Re}\int_{4m_\pi^2}^\infty ds \frac{R(s)}{\mathrm{s}(s-M_Z^2-i\epsilon)} \quad (2)$$

where the kernel $\hat{K}(s)$ is a smooth bounded function growing from 0.63 at threshold to 1 at ∞.

The contribution expected by DAΦNE will be discussed separately for each quantity.

1.0.1 Contribution of DAΦNE to a_μ^{had}

In an updated analysis [2] using the existing e^+e^- data in the region below 40 GeV, a value of $a_\mu^{had} = (7023 \pm 153)\cdot 10^{-11}$ has been found. DAΦNE can reduce this error, since the low energy contributions to a_μ^{had} are enhanced by the presence of the $1/s^2$ term in the integral of Eq. 2.

In particular the range of energies below 1.4 GeV accounts for 77% of the total quadratic error, the ρ resonance region being responsible for 62% of it. A measurement of the hadronic cross section up to 1.4 GeV at the 1% level of accuracy would allow to reduce δa_μ^{had} to $\sim 70 \cdot 10^{-11}$ [1, 2, 4], which could be further reduced to $\sim 15 \cdot 10^{-11}$ by achieving the same accuracy in the range $[1.40 \div 3.10]$ GeV.

This measurement is particularly intriguing in the light of the new $(g-2)$ experiment at BNL which has started to collect data in 1997 and it is supposed to achieve the goal of $35 \cdot 10^{-11}$ for the measurement of a_μ [5]. With this measurement and with the new data from DAΦNE it will be possible to achieve an accuracy on a_μ to isolate the electroweak contribution ($a_\mu^{EW} = 151 \pm 4 \cdot 10^{-11}$) at more than 2σ level. Of particular interest [6] will be the possibility to put a new stringent limit on

[1] $\Delta\alpha^{had}(M_Z^2)$ is the hadronic part of $\Delta\alpha(M_Z^2)$, related to $\alpha(M_Z^2)$ and to the fine constant α by $\alpha(s) = \frac{\alpha(s)}{1-\Delta\alpha(s)}$.

the gauge boson anomalous coupling, $|\Delta k_\lambda| \leq 0.2$, a factor 10 better of the actual experimental values obtained at the FermiLab Collider.

1.0.2 Contribution of DAΦNE to $\Delta\alpha^{had}(M_Z^2)$

Different from a_μ^{had}, $\Delta\alpha^{had}(M_Z^2)$ has contributions mainly from energies higher than the DAΦNE range [2]. Although the total error can be reduced by an order of magnitude by accurate measurements of hadronic cross sections in the interval $4m_\pi^2 < s < M_\Upsilon$, only about 10% comes in the region around the ρ resonance. For this reason a measurement of $\sigma(e^+e^- \to hadrons)$ in the range below to 2 GeV is not so crucial for this quantity.

A different approach [2, 7] has been recentely proposed to evaluate $\Delta^{had}\alpha(M_Z^2)$. Based on the evaluation of the so called Adler function, it allows to use *safely* pQCD down to about 2.5 GeV *plus* experimental data up to that threshold:

$$\Delta^{had}\alpha(-M_Z^2) = \left[\Delta^{had}\alpha(-M_Z^2) - \Delta\alpha^{had}(-(2.5GeV)^2)\right]^{pQCD} + \Delta\alpha^{had}(-(2.5GeV)^2)_{data}$$

Since the error on the non-perturbative "remainder" $\Delta\alpha^{had}(-(2.5GeV)^2)_{data}$ is dominated by the energies below the J/ψ, an accuracy of 1% on $\sigma(e^+e^- \to hadrons)$ up to the J/ψ could allow to reduce the actual error on $\Delta^{had}\alpha(-M_Z^2)$ by about 70%.

In this approach DAΦNE could play an important role, since the energies below the ϕ contribute with more than 40% to $\Delta\alpha^{had}(-(2.5GeV)^2)_{data}$ and to the corresponding error.

2 Measuring $\sigma(e^+e^- \to hadrons)$ using a tagged photon

Since DAΦNE should run at fixed energy for at least the next 2 years, a scanning of the beams is not foreseen at short term. An alternative approach to change the energy of the hadrons while DAΦNE operates at $\sqrt{s} = M_\phi$ is offered by the radiative process $e^+e^- \to hadrons + \gamma$, where the γ is emitted in the initial state (*i.s.r.*) [8].

The differential cross section for the emission of a photon of energy E_γ and polar angle larger than θ_0 from the initial state can be written as [8]:

$$\frac{d\sigma}{dQ^2} = \sigma_{e^+e^-\to hadrons}(Q^2) H(Q^2, s, \cos\theta_0) \qquad (3)$$

where Q^2 is the invariant mass of the hadronic system, related to E_γ by $Q^2 = s - 2\sqrt{s}E_\gamma = M_\phi^2 - 2M_\phi E_\gamma$ and $H(Q^2, s, \cos\theta_0)$ is the radiating function describing the emission of the hard photon with angles bigger then θ_0, peaked itself at small θ_0.

Eq. 3 shows why it is possible to use $i.s.r$ events to get information on $\sigma_{e^+e^-\to hadrons}$ for a quite wide range of energies, $4m_\pi^2 \leq Q^2 < M_\phi^2$.

As a simple application of this method the hadronic contribution to (g-2), a_μ^{had}, can be obtained by combining Eqs. 2 and 3 [2]:

$$a_\mu^{had} = \frac{1}{4\pi^3}\int_{4m_\pi^2}^{Q^2_{max}} dQ^2 \sigma_{e^+e^-\to\pi^+\pi^-}(Q^2)K(Q^2) = \int_{4m_\pi^2}^{Q^2_{max}} d\sigma_{e^+e^-\to\pi^+\pi^-\gamma}(Q^2)\frac{K(Q^2)}{H(Q^2, s, \cos\theta_0)} \tag{4}$$

where $K(Q^2) = m_\mu^2/3Q^2\hat{K}(Q^2)$.

In order to obtain an expression more practical to use experimental data, the above integral can be approximated by a sum over a finite set of intervals Q_i^2 in the range $4m_\pi^2 \leq Q_i^2 \leq Q^2_{max}$; in that case a_μ^{had} takes the form:

$$a_\mu^{had} = \frac{1}{L}\sum_{i=1}^{N}\frac{K_i}{H_i}N_i \tag{5}$$

where N_i is the number of events counted in the *i-th* interval of Q^2 and L is the integrated luminosity. A small bin size is clearly required in order to reduce as much as possible the error in the approximation of the integral. Eq. 5 translates the required accuracy of a_μ^{had} into a precise counting of $\pi^+\pi^-\gamma$ events: in the following we assume a relative accuracy of 1% for a single bin as our goal. This challenging task will require, among others, a good resolution and precise alignment of the detector, a very good knowledge of the absolute normalization, and from the theoretical side an accurate evaluation of high order corrections.

It's important to note that, due to the constraint $Q^2 = M_\phi^2 - 2M_\phi E_\gamma$, a binning on Q^2 is equivalent to a binning on E_γ, and an expression similar to Eq. 5 can be derived as a function of the population in the *i-th* bin of E_γ [9].

Assuming in particular a threshold for E_γ of 50 MeV (as will be motivated in the following), Eq. 5 allows to explore the following energy range:

$$0.050\,\mathrm{GeV} \leq E_\gamma \leq 0.470\,\mathrm{GeV} \Longleftrightarrow 0.077\,\mathrm{GeV}^2 \leq Q^2 \leq 0.938\,\mathrm{GeV}^2 \tag{6}$$

Which one of these two variables will be chosen depends on the experimental set up; in our case the possibility to measure independently the energy of the photon with

[2] We will now focuse on the final state $\pi^+\pi^-\gamma$, being $\pi^+\pi^-$ the most relevant hadronic channel below the ϕ.

the Electromagnetic Calorimeter ($EMCAL$) and the invariant mass of the charge pions with the Drift Chamber (DC) allows in principle to use both options.

An analysis based on the detection of the radiated photon with the KLOE calorimeter has been discussed in [9]. In that paper it has been shown that the finite resolution of the calorimeter represents a problematic effect, in order to achieve the required accuracy of a_μ^{had}, and requires a deconvolution procedure.

Our strategy, on the contrary, will be based on the measurement of Q^2 of the two pions with the drift chamber which indirectly allows to retrieve E_γ, as discussed above. This quite different approach provides a considerably better resolution for E_γ (as shown in Fig. 12) and a larger acceptance of the tagged photon (down to 10^o).

3 $\pi^+\pi^-\gamma$ identification procedure

Since the KLOE detector doesn't allow to tag γ from the initial state radiation (*i.s.r.*) below 7^o (or above 173^o [3]), where the contribution from the final state radiation (*f.s.r.*) can be neglected, a detailed simulation of both initial and final state radiation processes is required. A Monte Carlo event generator of $\pi^+\pi^-\gamma$ events [10] (including *i.s.r.*, *f.s.r.* and collinear radiation) has been interfaced with the detector simulation program GEANFI [4]. The full reconstruction procedure has been applied to the simulated events.

In Tab. 1 the Monte Carlo total cross section (*i.s.r.* plus *f.s.r.*) integrated over the photon polar angle $\sigma = \int_{\theta_\gamma^{min}}^{\theta_\gamma^{max}} \frac{d\sigma}{d\theta_\gamma} d\theta_\gamma$ is computed as a function of θ_γ^{min} (given in the rows) and θ_γ^{max} (given in the columns).

A symmetric cut is applied on the polar angle of the two pions, $20^o < \theta_{\pi^\pm} < 160^o$.

In Tab. 2 the ratio between the cross section for *i.s.r.* and the integrated total cross section is shown for the same values of the photon polar angle.

As can be noted, it is most important to increase as much as possible the acceptance for small angles. Since the KLOE $EMCAL$ acceptance is drastically reduced below 20^o, the calorimeters surrounding the focusing quadrupoles ($QCAL$'s, covering the region $13^o < \theta < 20^o$; *and* $160^o < \theta < 167^o$) will be used. This will allow to increase our acceptance down to 10^o, as will be shown in the following.

[3] In the following we consider only one side of our detector, $\theta < 90^o$, since for the other side the results can be obtained simply translating $\theta \to \theta' = 180^o - \theta$.

[4] GEANFI release of 22.2.99.

$\sigma_{isr+fsr}$[nb]	**10°**	**20°**	**30°**	**40°**
7°	0.872 ± 0.006	2.60 ± 0.02	3.65 ± 0.03	4.44 ± 0.03
10°	-	1.72 ± 0.02	2.77 ± 0.02	3.56 ± 0.03
20°	-	-	1.05 ± 0.01	1.83 ± 0.01
30°	-	-	-	0.789 ± 0.006

Table 1: Integrated total cross section as a function of θ_γ^{min} (given in the rows) and θ_γ^{max} (given in the columns), as expected from Monte Carlo.

$\frac{\sigma_{isr}}{\sigma_{isr+fsr}}$	**10°**	**20°**	**30°**	**40°**
7°	0.995 ± 0.01	0.99 ± 0.01	0.98 ± 0.01	0.97 ± 0.01
10°	-	0.98 ± 0.01	0.975 ± 0.01	0.96 ± 0.01
20°	-	-	0.955 ± 0.01	0.945 ± 0.01
30°	-	-	-	0.92 ± 0.01

Table 2: Ratio between the cross section for *i.s.r.* and the integrated total cross section as a function of θ_γ^{min} (given in the rows) and θ_γ^{max} (given in the columns) as expected from Monte Carlo.

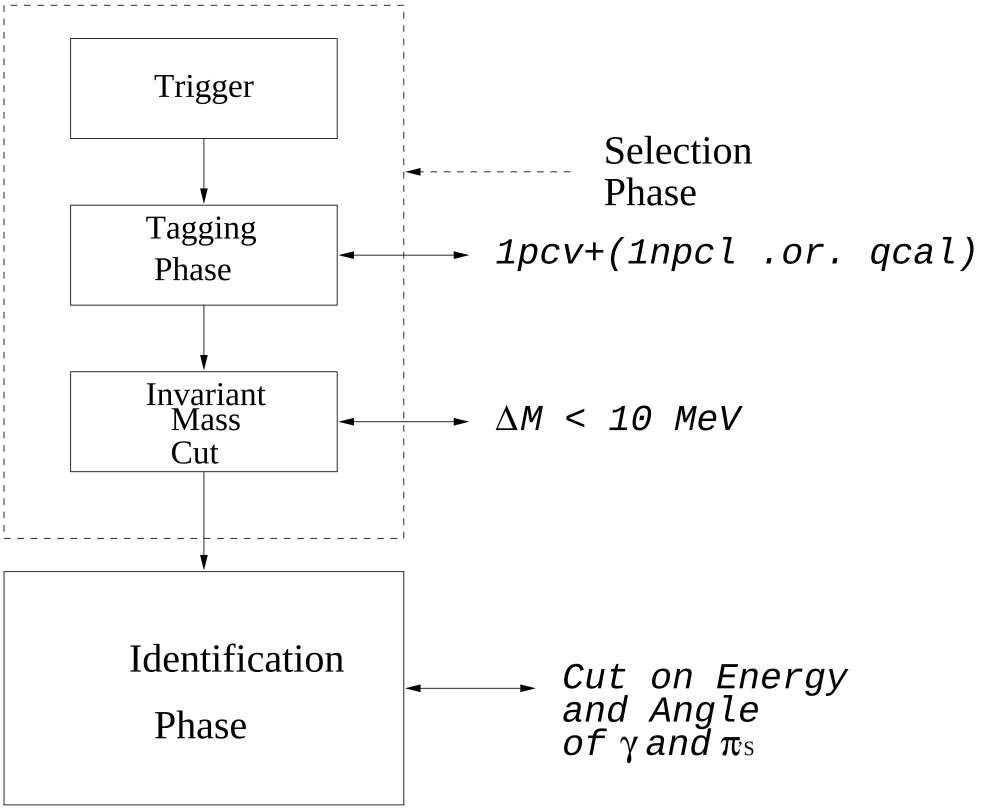

Figure 1: Scheme of the identification procedure. npcl = neutral prompt cluster; pcv = prompt charged vertex.

In order to select with high efficiency and low background $\pi^+\pi^-\gamma$ events from *i.s.r.*, the identification procedure will be performed in two steps:

1. in a first step $\pi^+\pi^-\gamma$ events will be selected, according to their clearly defined signature. In this phase also events from *f.s.r.* can be accepted;

2. in a second step a favoured kinematical region of energies and angles of pions and photons will be selected in order to reduce as much as possible the *f.s.r.*, as well as other possible contaminations.

Fig. 1 shows a scheme of the identification procedure.

3.1 The selection phase

The existence of a charged vertex (*pcv*) close to the interaction region with an associated photon is the basic requirement to tag $\pi^+\pi^-\gamma$ events [11]. However, different from the vertex efficiency, the photon acceptance depends on the direction of the γ, especially at low θ. This behaviour can be seen in the upper plot of Fig. 2, in which the efficiency to reconstruct a prompt neutral cluster (*npcl*) is plotted as a function of the Monte Carlo polar angle of γ. In order to increase the acceptance at small angles, the information from the $QCAL$ has to be considered. Fig. 3 plots the energy deposition and the mean time, averaged over the energy in a $QCAL$ detector for $\pi^+\pi^-\gamma$ events, with $\theta_\gamma > 10^o$. An efficient tagging condition can be defined by selecting events for which the total energy is between 0.1 and 20 MeV, with a corresponding time between 7 and 11 ns.

In the central plot of Fig. 2 the tagging efficiency so obtained from the $QCAL$ is plotted as a function of the γ polar angle: as can be noted, the maximum efficiency, $\sim 90\%$, is obtained in the region between $\sim 13^o$ and $\sim 19^o$, corresponding to the nominal position of one detector. In the same figure (Fig. 2(down)), the efficiency obtained by combining the information from the $EMCAL$ and the $QCAL$ is plotted: as can be noted, the efficiency for $\theta_\gamma > 10^o$ is $\sim 90\%$ and almost flat.

As the final step of the tagging phase a constraint on the invariant mass is applied in order to reject as much as possible the background events (as for example $e^+e^- \to \mu^+\mu^-\gamma$). In Fig. 4 the quantity $\Delta M = M_\phi - \sqrt{|\vec{p}_+|^2 + m_\pi^2} - \sqrt{|\vec{p}_-|^2 + m_\pi^2} - |\vec{p_\phi} - \vec{p}_+ - \vec{p}_-|$, where $\vec{p_\pm}$ are the reconstructed momenta of the charged tracks associated with the selected vertex and $\vec{p_\phi}$ is the momentum of the ϕ (12.5 MeV/c in the x direction), is compared for the wanted signal and two relevant backgrounds: $\phi \to \pi^+\pi^-\pi^0$ and $e^+e^- \to \mu^+\mu^-\gamma$. [5] The chosen cut $|\Delta M_\phi| < 10\,\mathrm{MeV}$ is also shown.

The tail of the $\pi^+\pi^-\gamma$ distribution consists of events in which a collinear photon is also emitted, together with the hard photon in the initial state (*collinear radiation*). The rejection of these events, which in principle could be selected by an asymmetric cut [11], is necessary to avoid a systematic error in the reconstruction of the extrapolated energy and direction of the photon, which is obtained by momenta conservation:

$$E_\gamma = |\vec{p_\phi} - \vec{p_+} - \vec{p_-}|$$

Unfortunately not all the collinear radiation events give raise to the tail of Fig. 4: indeed in a part of these events the photons are emitted in such a kinematical configuration that their total energy is very close to the modulus of their total

[5] An arbitrary normalization has been considered.

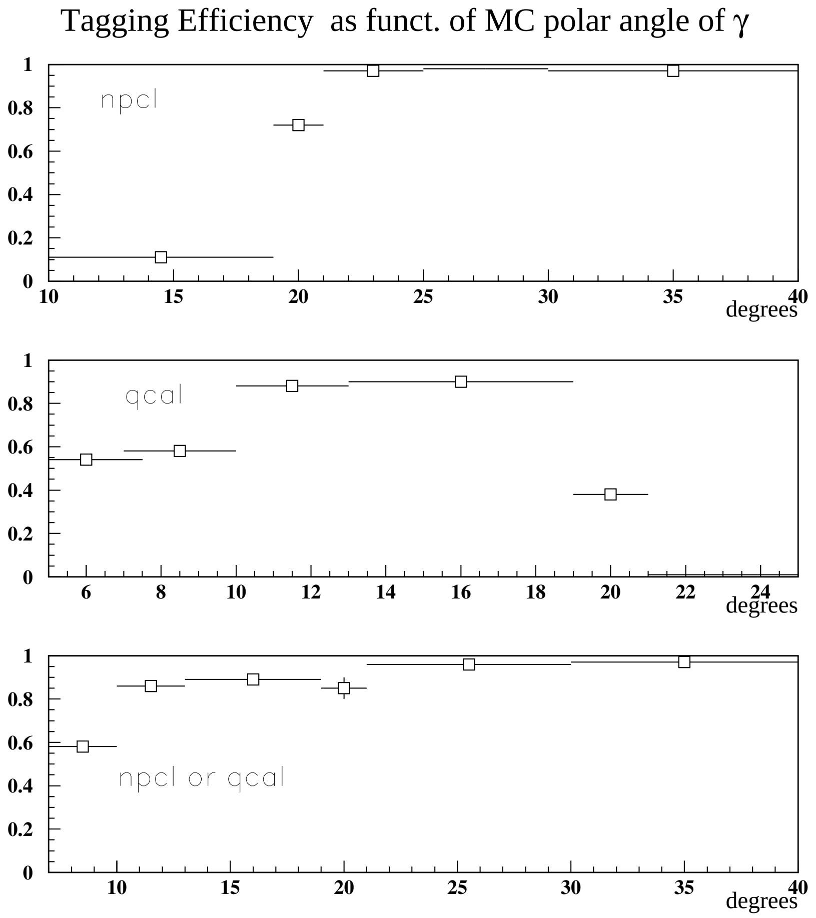

Figure 2: Photon tagging efficiency as a function of the Monte Carlo θ_γ:(up) *npcl* efficiency; (centre) $QCAL$ efficiency; (down) *npcl* and $QCAL$ combined efficiency. (Details are given in the text.)

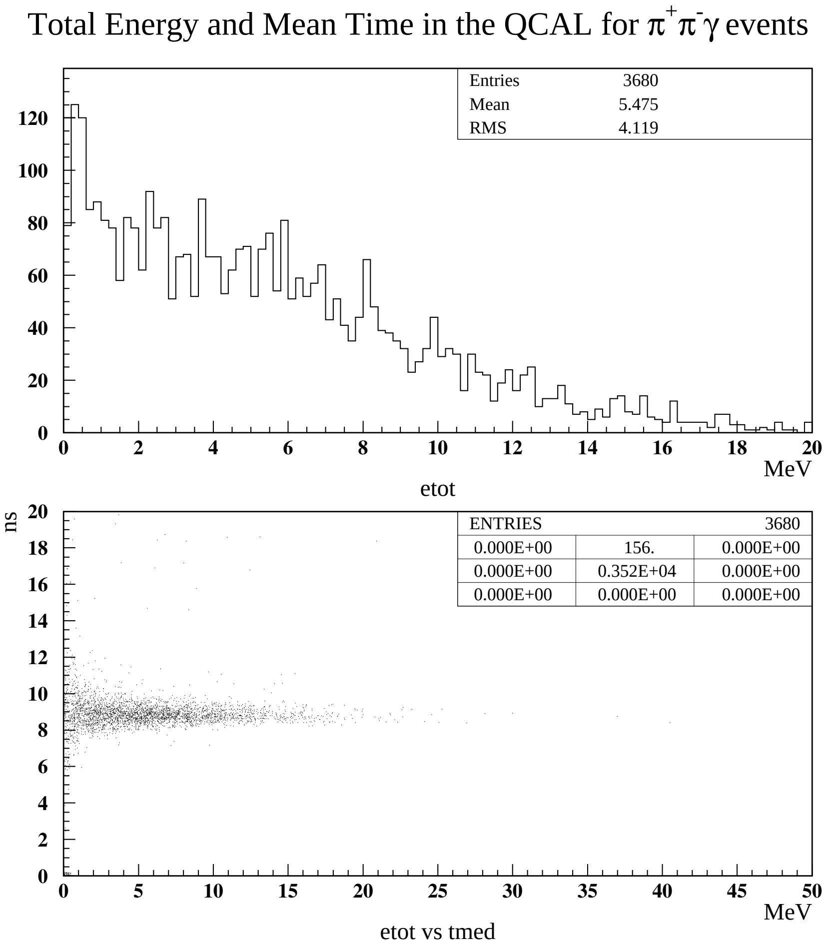

Figure 3: (up) Energy deposition and (down) average time of a $QCAL$ detector for $\pi^+\pi^-\gamma$ events, with $\theta_\gamma > 10^o$.

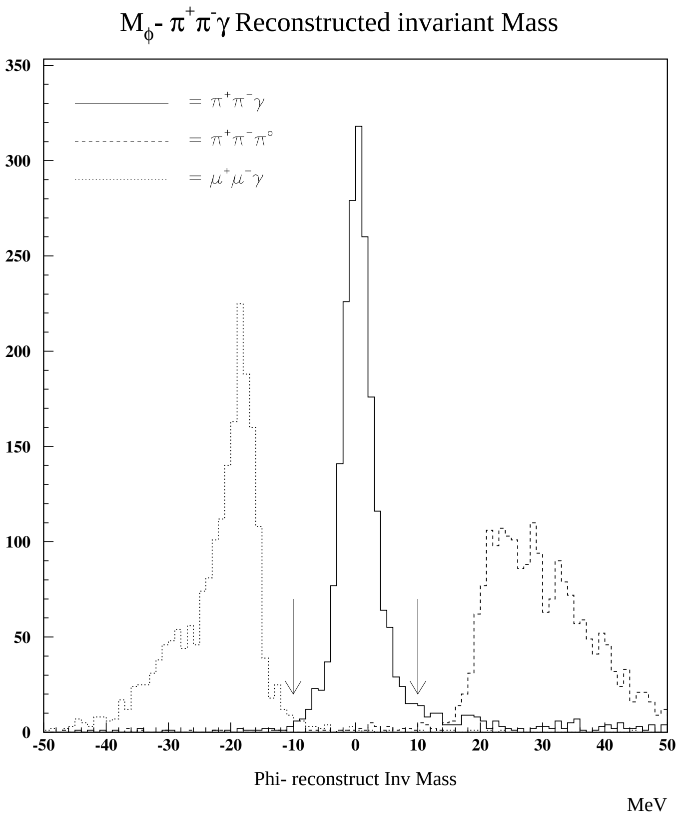

Figure 4: $\Delta M = M_\phi - \sqrt{|\vec{p}_+|^2 + m_\pi^2} - \sqrt{|\vec{p}_-|^2 + m_\pi^2} - |\vec{p_\phi} - \vec{p}_+ - \vec{p}_-|$ for three different samples. The arrows show the cut $|\Delta M| < 10 MeV$.

momentum, giving therefore a negligible contribution to ΔM. These undesired events will survive the cut $|\Delta M_\phi| < 10\,\mathrm{MeV}$ and they will be expected to worsen the resolution on E_γ (as will be shown in the following).

The final selection efficiency combining all the above cut is $\sim 80\%$, becoming $\sim 65\%$ by introducing also the KLOE trigger filter (the inefficiency being mostly due to cosmic veto).

3.2 The identification phase

In the previous phase $\pi^+\pi^-\gamma$ events are selected no matter of the "real nature" of the emitted photon (*i.s.r* or *f.s.r*). These different processes, which lead to the same final state, can be however discriminated by looking at the following quantities:

- The angle of the emitted photon θ_γ. Differently from *i.s.r*, strongly peaked at small angle, the contribution of *f.s.r* increases proportionally with θ_γ, as can be seen in Fig. 5 (or in Tab. 2), and therefore can be reduced by requiring small θ_γ. However, as previously discussed, θ_γ can't be reduced to any desirably small angle without compromising on the photon tagging efficiency (see Fig. 2). More important is the *flatness* of such an efficiency, which is obtained above 10^o. However, as can be noted in Tab. 2 a relevant contribution of *f.s.r* is expected above that threshold ($\sim 4\%$ in the region $10^o < \theta_\gamma < 40^o$).

- The energy of the photon, E_γ, or equivalently the invariant mass of the two pions, Q^2. While *f.s.r.* is peaked at low energy, *i.s.r* is enhanced by the ρ resonance, $\sqrt{Q^2} = 0.770 GeV$ corresponding to $E_\gamma \sim 220\,\mathrm{MeV}$, as shown in Fig. 5. A cut on $E_\gamma > 50\,\mathrm{MeV}$ allows to reduce the *f.s.r.* contribution to about 40% for $10^o < \theta_\gamma < 40^o$.

The rejection factor for *f.s.r* can be further increased by combining together the cut on energy and polar angle of the photon, as shown in Fig. 6. The efficiency of this cut, which will be referred as **cut1**, will depend on the selected angular region (for istance $10^o < \theta_\gamma < 40^o$ in Fig. 6).

A more sophisticated cut can be obtained in the $\pi^-\gamma$ reference system (clearly similar considerations hold in the $\pi^+\gamma$'s one). In that system a quite different distribution of the angle between the transformed momentum of the photon (k') and the boost direction is expected for *i.s.r.* w.r.t. *f.s.r*, due to the different spectrum of E_γ. In particular, a high rejection factor of *i.s.r.* vs *f.s.r* can be achieved by looking at the correlation between E_γ and the angle Ψ between the direction of k' and of

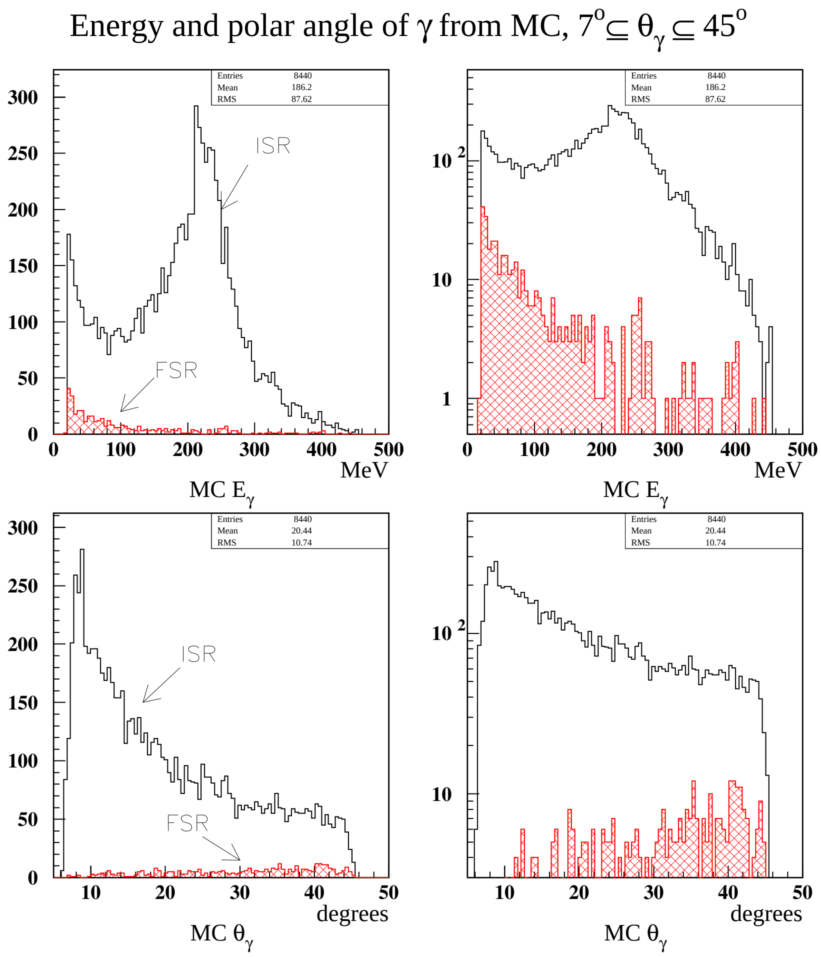

Figure 5: Distribution of energy and polar angle of the photon. The contribution of *f.s.r.* is emphasized by the logaritmic scale.

Angle vs Energy of γ from Monte Carlo

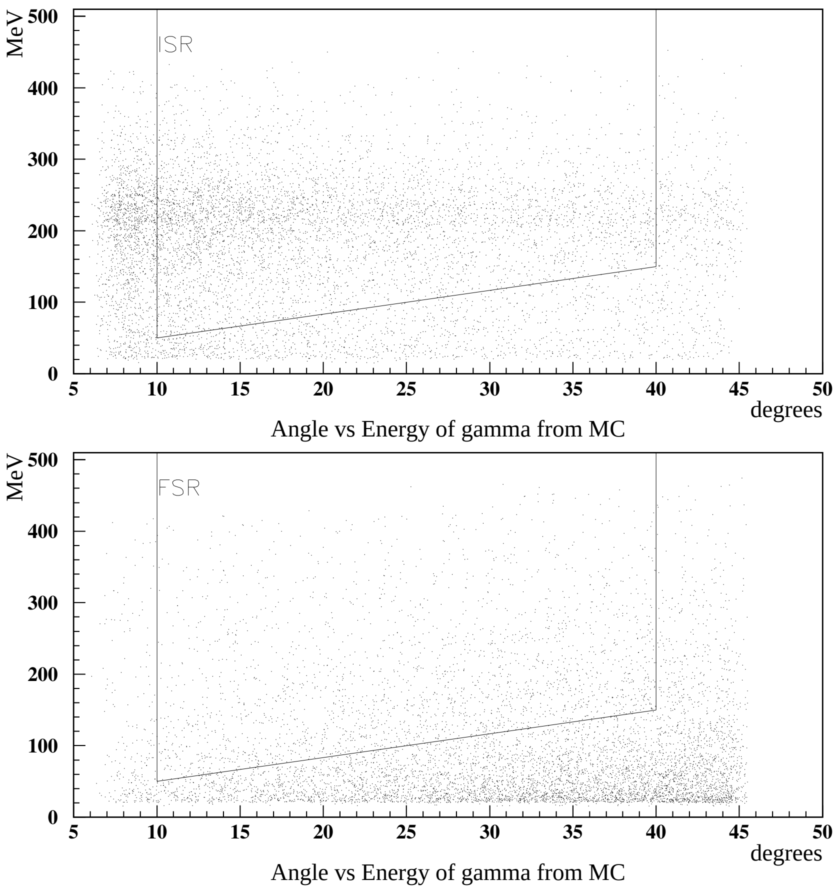

Figure 6: Correlation between energy and polar angle of the photon for $i.s.r$ (up) and $f.s.r$ (down). A possible cut is shown.

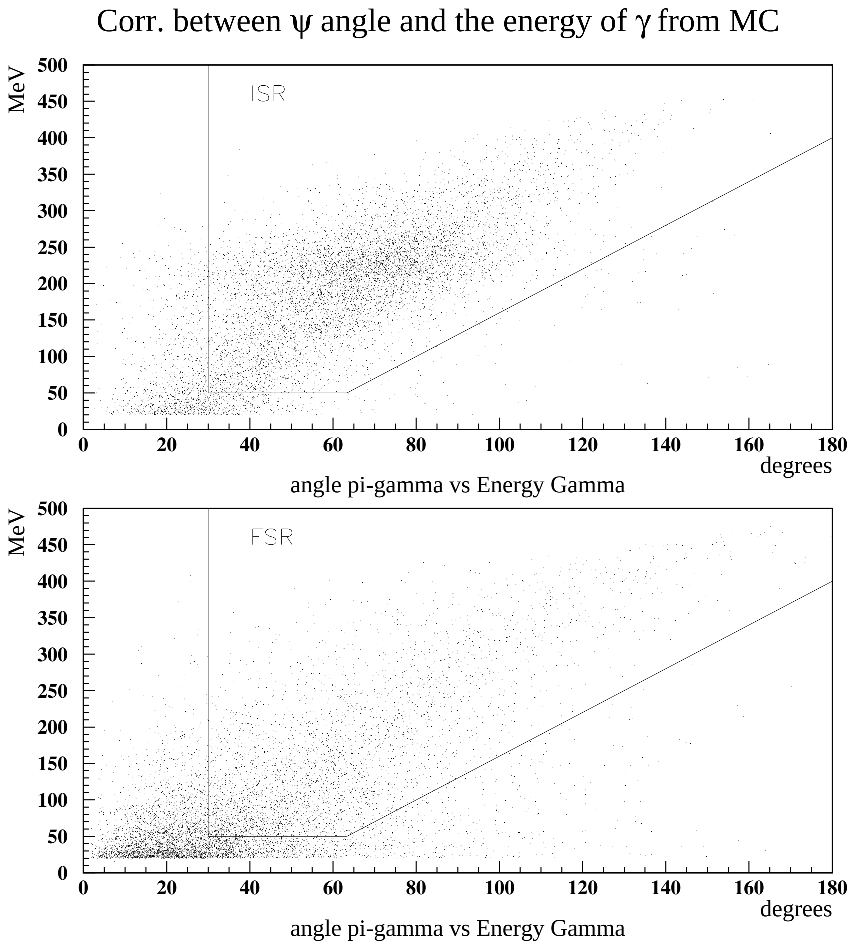

Figure 7: Scatter plot of E_γ and Ψ angle for *i.s.r.* (up) and *f.s.r* (down). The cut is indicated by the line. Details are given in the text.

the other pion (π^+ in our case). Such a correlation is shown in Fig. 7 for initial and final state radiation events, together with our optimized cut (which it will be referred as **cut2**).

The selection efficiencies for **cut1** and **cut2** will be given in the following section.

3.3 Resolution studies and selection efficiencies

In order to apply the identification procedure to the reconstructed events, preliminary studies on angular and energy resolution have been performed [6].

Fig. 8 shows the angular and energy resolutions for π^+ and π^-: resolutions less than 3 mrad and 1 MeV are expected for the polar angle and for the energy of reconstructed pions respectively. Such extremely good values allow to expect a very good resolution of the direction of the total momentum of the two pions (θ_{Q^2}) and of their total invariant mass, as well as of the extrapolated direction and energy of the photon, obtained by momentum conservation:

$$\vec{p_\gamma} = \vec{p_\phi} - \vec{p_+} - \vec{p_-}$$

Fig. 9 shows the obtained resolutions. The following considerations are opportune:

- the gaussian tail of the polar angle is mostly made of low energy photons with almost collinear pion tracks;
- the asymmetric tail in the distribution of the photon energy has two different sources: (a) the presence of collinear radiation, which gives raise to a gaussian tail and (b) the cut on ΔM which rejects only a part of these multiphoton events as can be noted by comparing the solid line distribution (normal selection) with the dotted one (obtained by removing this cut). By switching off the collinear radiation, the tail disappears, as can be seen in the shaded region of the same figure;
- since Q^2 is directly measured, it is not affected by the collinear radiation.

While the θ_γ and θ_{Q^2} resolutions are quite similar, the distributions for E_γ and Q^2 are differently affected by the various cuts. These differences are evidenced in Fig. 10, where the relative resolutions of E_γ and Q^2 are compared, together with the effects of the cuts on the invariant mass and the presence of the collinear radiation.

[6] When the distributions are fitted with two gaussians, the mean value and σ are taken from the gaussian with the highest number of events.

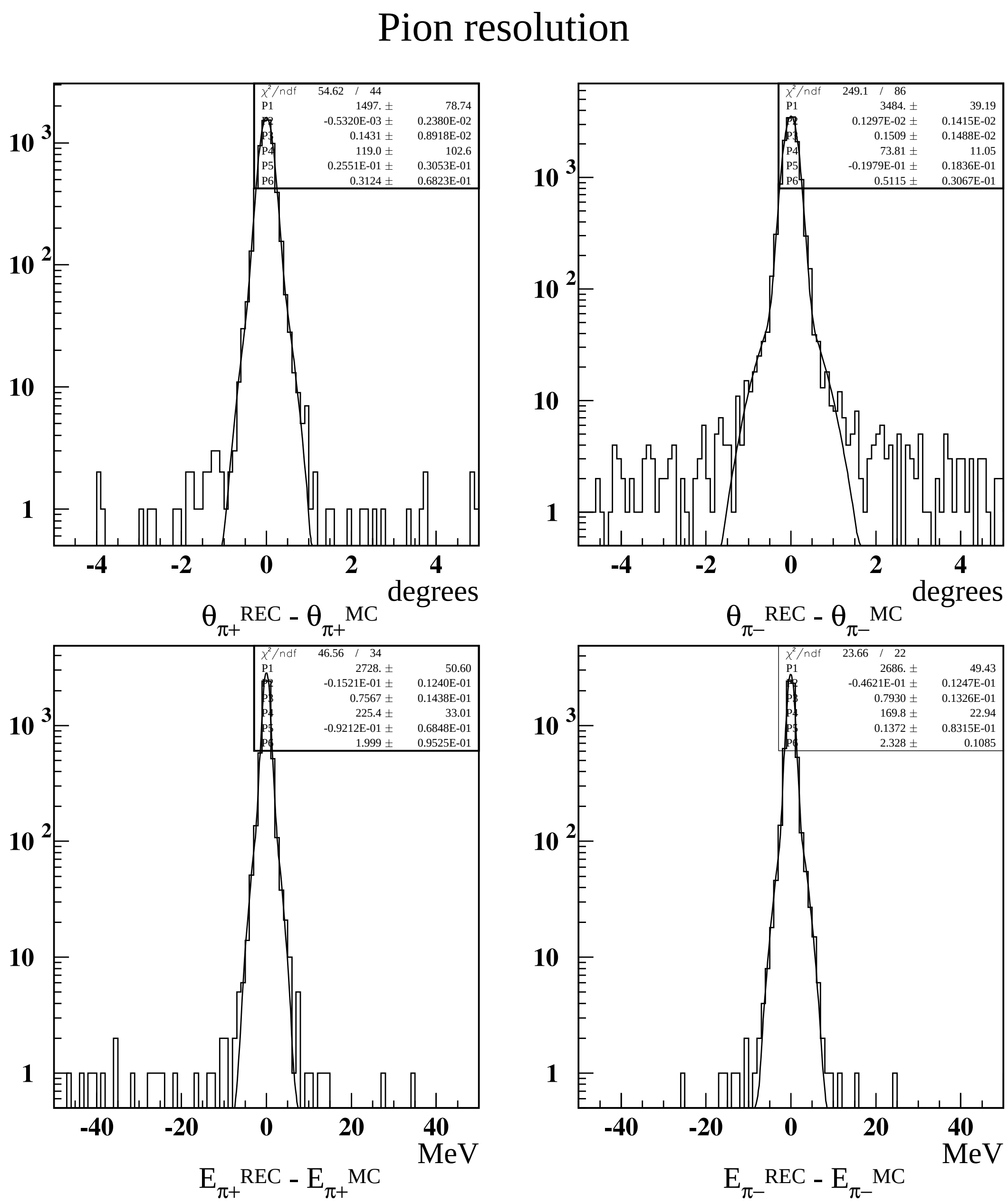

Figure 8: Angular and energy resolution for pions.

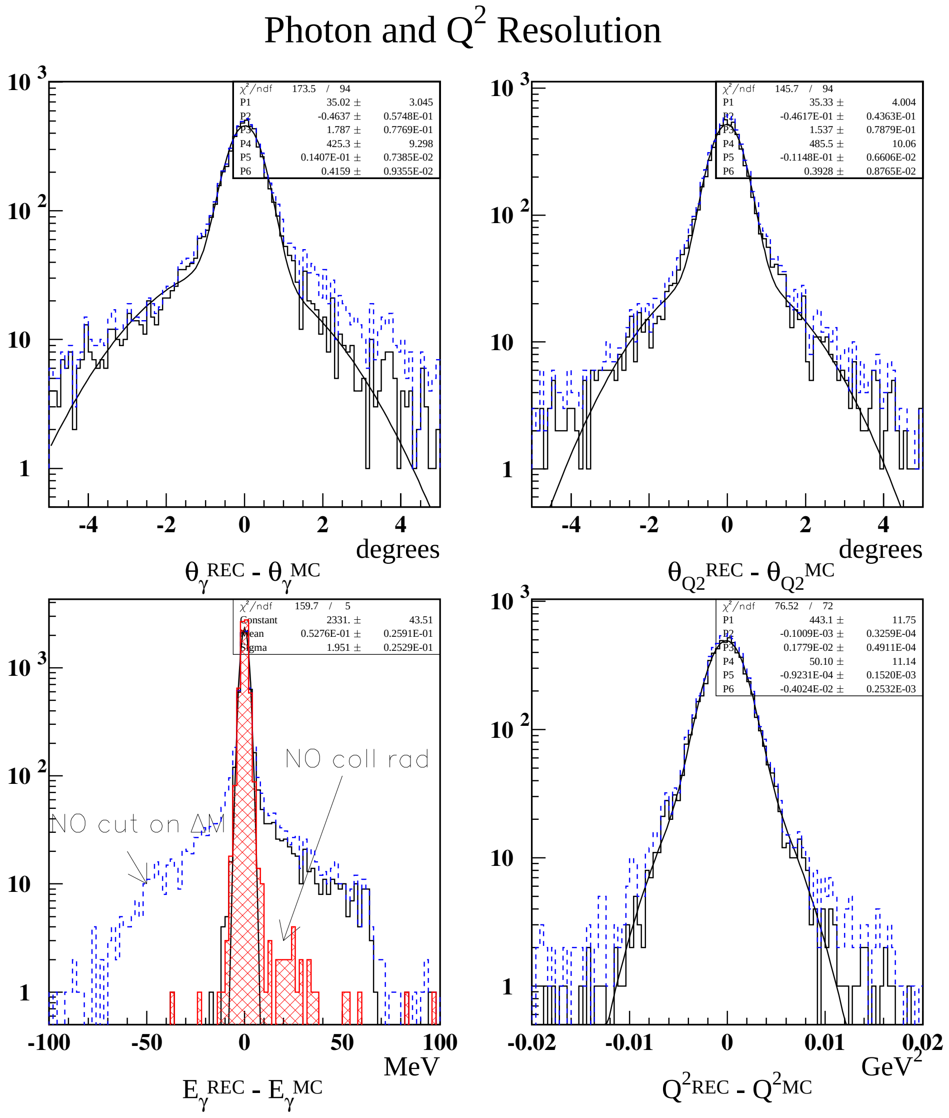

Figure 9: Angular and energy resolution for the two pion system and for the photon. In dotted line are shown the distributions with no cut on ΔM. Details are given in the text.

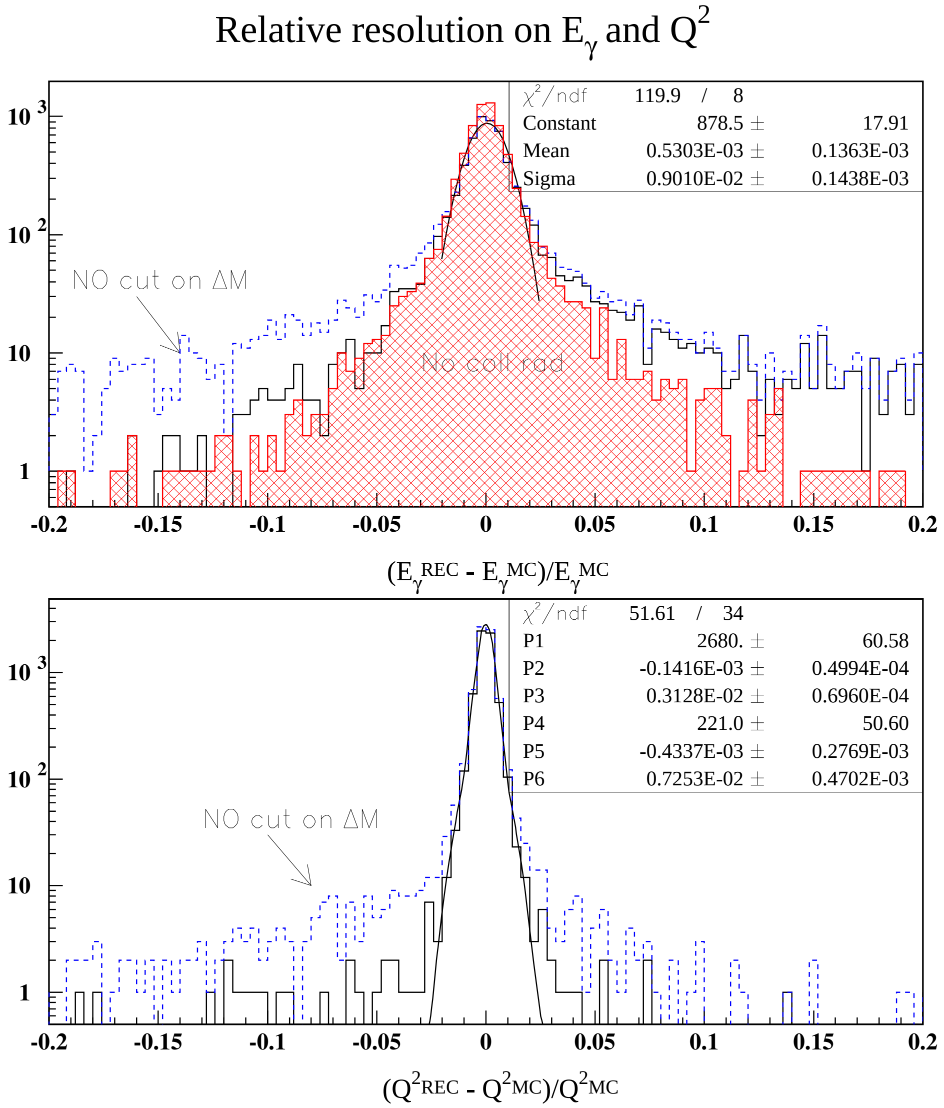

Figure 10: Fractional resolution on E_γ and Q^2. Dotted lines are obtained with no cut on ΔM.

As can be noted the variable Q^2 should be preferred above to E_γ since is provides a better resolution, and is not affected by the invariant mass cut or by the presence of the collinear radiation.

In Fig. 11 the resolutions of the angles θ_γ and Ψ are compared: these resolutions are only slightly affected by the two effects discussed.

Resolutions
$\sigma_{\theta_\pi} \sim 3mrad$
$\sigma_{E_\pi} \sim 1MeV$
$\sigma_{\theta_\gamma} \sim 7mrad$
$\sigma_{\theta_{Q^2}} \sim 7mrad$
$\sigma_{E_\gamma} \sim 2MeV$
$\sigma_{Q^2} \sim 2 \times 10^{-3} GeV^2$
$\sigma_{E_\gamma}/E_\gamma \sim 1\%$
$\sigma_{Q^2}/Q^2 \sim 0.3\%$
$\sigma_\Psi \sim 7mrad$

Table 3: Resolutions obtained for $\pi^+\pi^-\gamma$ events.

In Tab. 3 the obtained resolutions are summarized. As result of the previous discussion Q^2, θ_γ and Ψ will be used for the selection of *i.s.r.* events. More important, the energy scan and the interval partition will be done in Q^2.

In order to compare the cross sections and *f.s.r.* contamination at the end of the identification procedure for the two different cuts, **cut1** and **cut2**, their dependence on E_γ has been translated into Q^2.

Tab. 4 and 5 compare the integrated total cross section and the relative contribution of *i.s.r* in the reconstructed $\pi^+\pi^-\gamma$ events for cuts **cut1** and **cut2**. Although the cut efficiency (combined with the results of the selection phase) is for both cuts $\sim$ 50% (by comparing with Tab. 1 and 2), **cut2** provides a slightly better *f.s.r.* rejection factor. In particular, by using **cut2**, our identification procedure provides a total cross section of about $3.7nb$ (on both sides of the detector) of $\pi^+\pi^-\gamma$ *i.s.r.* events with an acceptable contamination from *f.s.r.* of the order of 1%, in the angular region $10^o < \theta_\gamma < 40^o$ *or* $140^o < \theta_\gamma < 170^o$. This choice will be implemented in the identification phase of our algorithm.

In principle other strategies can be explored, and other powerful variables can be found. An alternative possibility concerns the direct measurement of the energy

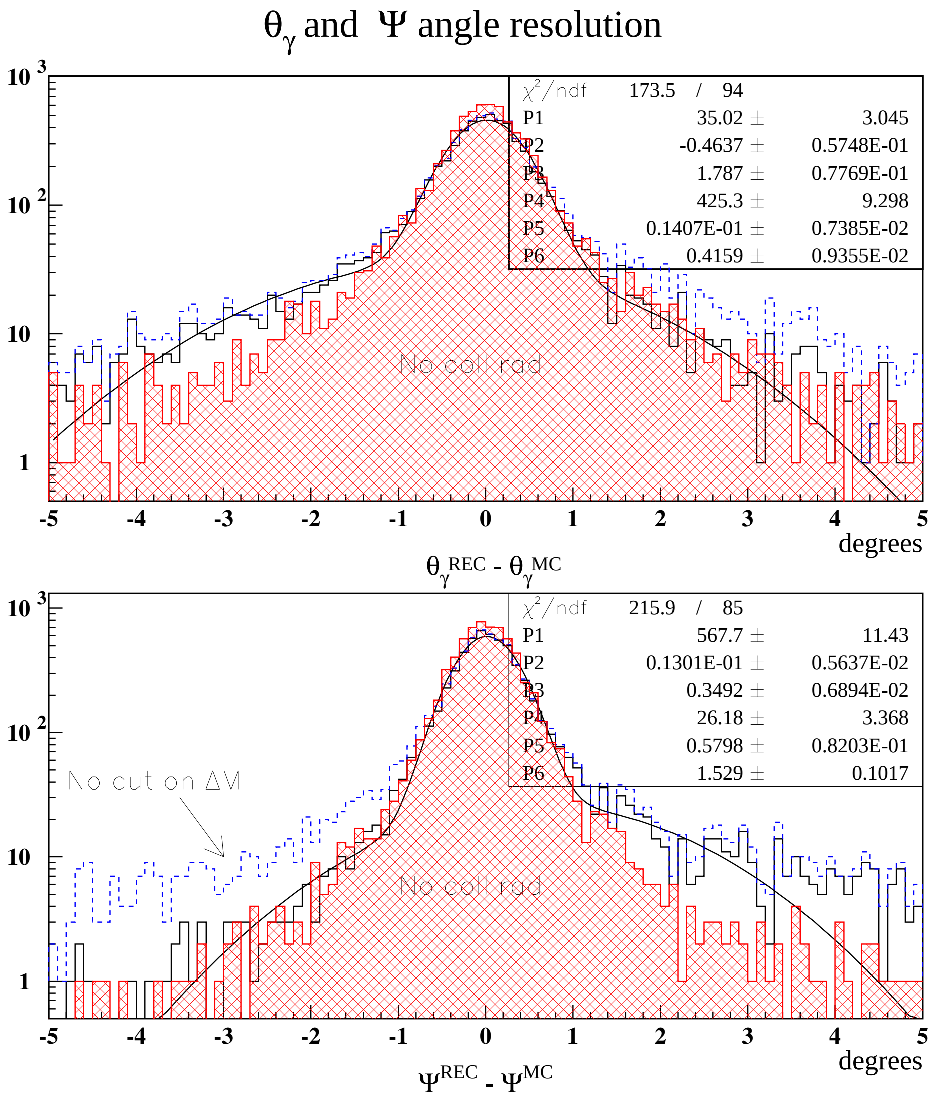

Figure 11: θ_γ and Ψ angle resolution. Dotted lines are obtained with no cut on ΔM. Shaded distributions are obtained without colliner radiation.

cut1				
$\sigma_{isr+fsr}[nb]$	**10°**	**20°**	**30°**	**40°**
7°	0.52 ± 0.008	1.55 ± 0.01	2.07 ± 0.02	2.43 ± 0.02
10°	-	1.04 ± 0.01	1.56 ± 0.015	1.92 ± 0.02
20°	-	-	0.52 ± 0.008	0.88 ± 0.01
30°	-	-	-	0.36 ± 0.006
$\frac{\sigma_{isr}}{\sigma_{isr+fsr}}$	**10°**	**20°**	**30°**	**40°**
7°	0.97 ± 0.01	0.98 ± 0.01	0.98 ± 0.01	0.98 ± 0.01
10°	-	0.98 ± 0.01	0.98 ± 0.01	0.98 ± 0.01
20°	-	-	0.96 ± 0.01	0.98 ± 0.01
30°	-	-	-	0.97 ± 0.01

Table 4: Integrated total cross section and relative presence of *i.s.r.* for $\pi^+\pi^-\gamma$ reconstructed sample selected by **cut1**.

cut2				
$\sigma_{isr+fsr}$[**nb**]	**10°**	**20°**	**30°**	**40°**
7°	0.47 ± 0.008	1.44 ± 0.01	1.95 ± 0.02	2.33 ± 0.02
10°	-	0.96 ± 0.01	1.47 ± 0.015	$\mathbf{1.85 \pm 0.02}$
20°	-	-	0.50 ± 0.008	0.89 ± 0.01
30°	-	-	-	0.385 ± 0.006
$\frac{\sigma_{isr}}{\sigma_{isr+fsr}}$	**10°**	**20°**	**30°**	**40°**
7°	0.98 ± 0.01	0.98 ± 0.01	0.98 ± 0.01	0.98 ± 0.01
10°	-	0.99 ± 0.01	0.99 ± 0.01	$\mathbf{0.99 \pm 0.01}$
20°	-	-	0.99 ± 0.01	0.99 ± 0.01
30°	-	-	-	0.97 ± 0.01

Table 5: Integrated total cross section and relative presence of *i.s.r.* for $\pi^+\pi^-\gamma$ reconstructed sample selected by **cut2**.

of the gamma with the calorimeter, as has been investigated in [9]. This method however has not been adopted for the following two reasons:

- the calorimeter acceptance considerably drops below 20^o;
- a considerably worse energy resolution is obtained w.r.t. our method, as can be shown in Fig. 12.

In particular, the relevant impact of the detector resolution on the systematical errors, will be pointed out in the section devoted to the discussion of systematic errors.

A modification of our procedure can be easily done by removing the tag of the photon in the selection phase. This extension would allow to increase the acceptance for photons below 10^o. Hovewer, in that case, a much consistent background is expected, which in principle could be reduced to an acceptable level by a global fit. The investigation of this possibility is under study.

A final comment is at place on the role of E_γ and Q^2 in our procedure. In principle, as emphasized many times, it is possible to use E_γ instead of Q^2 to scan the hadronic cross sections. Although a worse resolution is expected, this choice could have some benefits. In that case the asymmetric tail on E_γ due to collinear radiation could be corrected by dropping the cut on invariant mass in the selection phase. However a different method should be found to reduce the backgrounds. This possibility is under study.

In the following the systematic errors and resolution effects will be studied both for Q^2 and E_γ distributions.

3.4 Background rejection

Apart from final state radiation, other processes, if not well identified, can simulate our signal. The most relevant are:

- $\phi \to \rho\pi - \pi^+\pi^-\pi^0$, when a photon is missed (with an *equivalent* $\sigma = 750nb$);
- $e^+e^- \to \mu^+\mu^-\gamma$ ($\sigma \sim 1\,nb$ for $7^o < \theta_\gamma < 45^o$);
- $\phi \to f_0\gamma \to \pi^+\pi^-\gamma$ decay. The B.R. for this decay cannot be easily predicted due to the not clear nature of the f_0 resonance. In the existing GEANFI simulation code [12], a $B.R.$ of $2.5 \cdot 10^{-4}$ is assumed for $\phi \to f_0\gamma$, equivalent to $\sigma \sim 1.3\,nb$. Work is going on to include a better treatment of the ϕ direct decay and it will be reported in a separate memo.

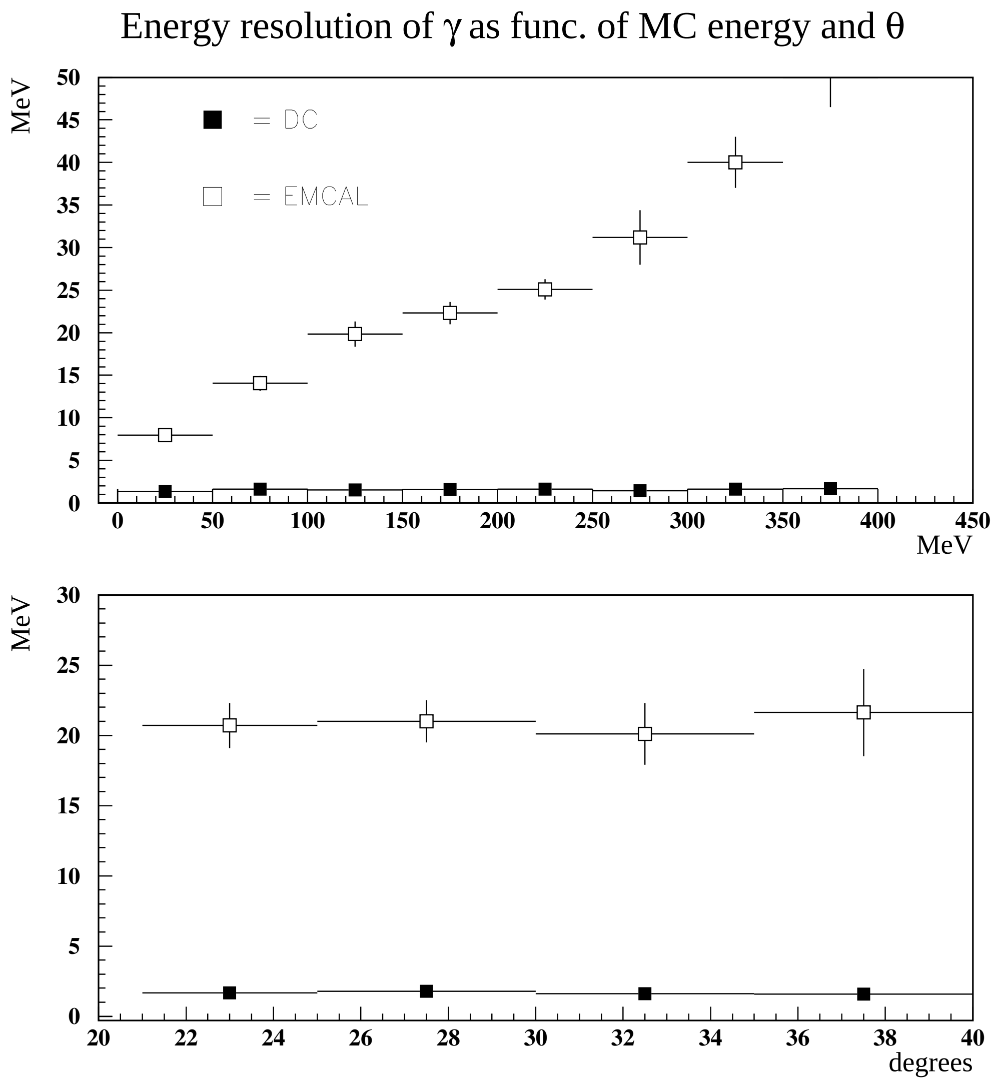

Figure 12: Comparison of the photon energy resolution measured directly with the calorimenter ($EMCAL$) and in our method (DC), as a function of the Monte Carlo energy (up) and polar angle of the photon (down).

	$\pi^+\pi^-\gamma$ *i.s.r.*	$\pi^+\pi^-\gamma$ *f.s.r.*	$f_0\gamma$	$\pi^+\pi^-\pi^0$	$\mu^+\mu^-\gamma$
σ (nb)	3.7	< 0.05	0.10	0.45	< 0.05
S/B	-	> 99	37	8	> 70

Table 6: Expected signal to background at the end of the identification procedure for different kinds of background.

Tab. 6 summarizes the expected cross sections at the end of the identification procedure and the ratio signal *over* background (S/B). The $\pi^+\pi^-\pi^0$ background, for which the contamination is still too high, is expected to be further reduced by a global fit. The $f_0\gamma$ contamination would be better estimated by a clearer understanding of f_0 resonance. The huge amount of $f_0 \to \pi^0\pi^0$ decays will be used for this aim [13].

4 Statistical errors

Fig. 13 [14] compares the required event yield to obtain $\delta a_\mu^{had} = 1.5 \cdot 10^{-10}$ with the one expected by assuming $\sigma_{i.s.r} = 3.7nb$ and a luminosity of $5 \cdot 10^{31} cm^{-2} sec^{-1}$ (a factor ten less then the design luminosity) As can be noted for such a luminosity statistics doesn't represent a problem.

5 Systematical error

Systematical errors in the evaluation of a_μ^{had} with Eq. 5 originate from the following sources:

1. The experimental values of energy and angle are different from the expected ones, due to a possible misalignment or wrong calibration of the detector, or of a not well known beam energy.

   In order to simulate such a systematic effect, a shift was "artificially" introduced on the beam energy and on the polar angle of the reconstructed photon:

$$\begin{aligned} E \to E' &= E + \Delta E \\ \theta_\gamma \to \theta'_\gamma &= \theta_\gamma + \Delta\theta \end{aligned}$$

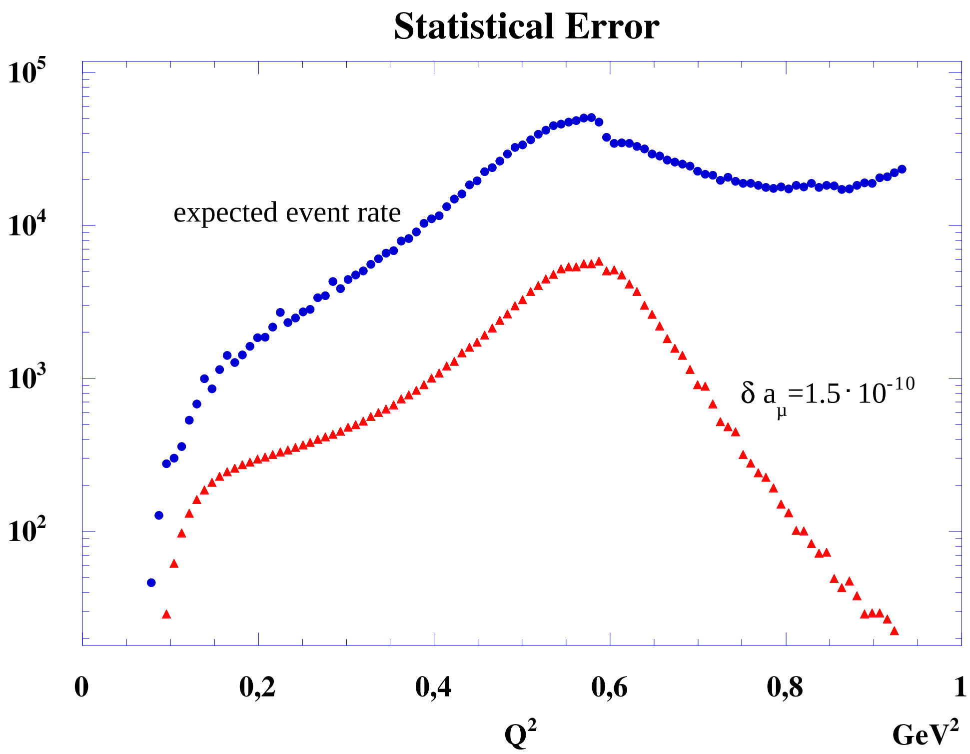

Figure 13: Comparison of the expected event rate (one year of data taking at a luminosity of $5 \cdot 10^{31} cm^{-2} sec^{-1}$) with the required number of events in order to achieve a statistical error of $\delta a_\mu^{had} = 1.5 \cdot 10^{-10}$.

Values of 0.5 MeV on the beam energy and of 3 mrad on $\Delta\theta$ (corresponding to a detector misalignment of 6 mm) have been found to give a relative error on the total cross section of the order of 1%.

The effect of these systematic shifts on the population of single bin of Q^2 and E_γ spectrum is shown in Fig. 14 and 15 for a 100 bins partition. The difference in population due to the shift, normalized to the nominal one (no shift), is given for each bin of energy. No worrying dependence on these shifts has been found.

2. The finite resolution of the detector, which affects the population of single bins as expected from Monte Carlo. The worse the resolution is, the more evident is the distortion of the spectrum of Q^2 (or E_γ).

   The comparison of the resolution in Q^2 and E_γ with the Monte Carlo calculations is shown in Fig. 16 and 17 respectively. With the good resolution, which is better for Q^2 than for E_γ (as already discussed), no drastic effects on the population of a single bin of energy is expected.

   This consideration can be confirmed by looking at Fig. 18, where the difference in population for the reconstructed and Monte Carlo data, normalized to the Monte Carlo ones, is given for each bin of energy. However the statistics should be incremented in order to precisely measure this effect.

   It is worthwile to note that the resolution effects would have a rather different impact on the direct measurement of E_γ with the calorimeter, as can be seen in Fig. 19. In that case a deconvolution procedure, as discussed in [9], must be applied.

3. An incorrect absolute normalization. In order to achieve the 1% level on the absolute event number, the luminosity must be known to the same level of accuracy. Such a task has been investigated in a dedicated KLOE Memo [15] and requires to use Bhabha events at large angles with a detailed simulation of higher order corrections. Work is going on in order to use the Bhabha generator provided by the Pavia group [16];

4. An uncertainty of the theoretical cross sections not larger than 1%. Such a nontrivial task requires an accurate evaluation of the higher order corrections and a precise description of the *f.s.r* process, taking into account in particular the interference with the contribution from the direct ϕ decay. Work is going in both these directions.

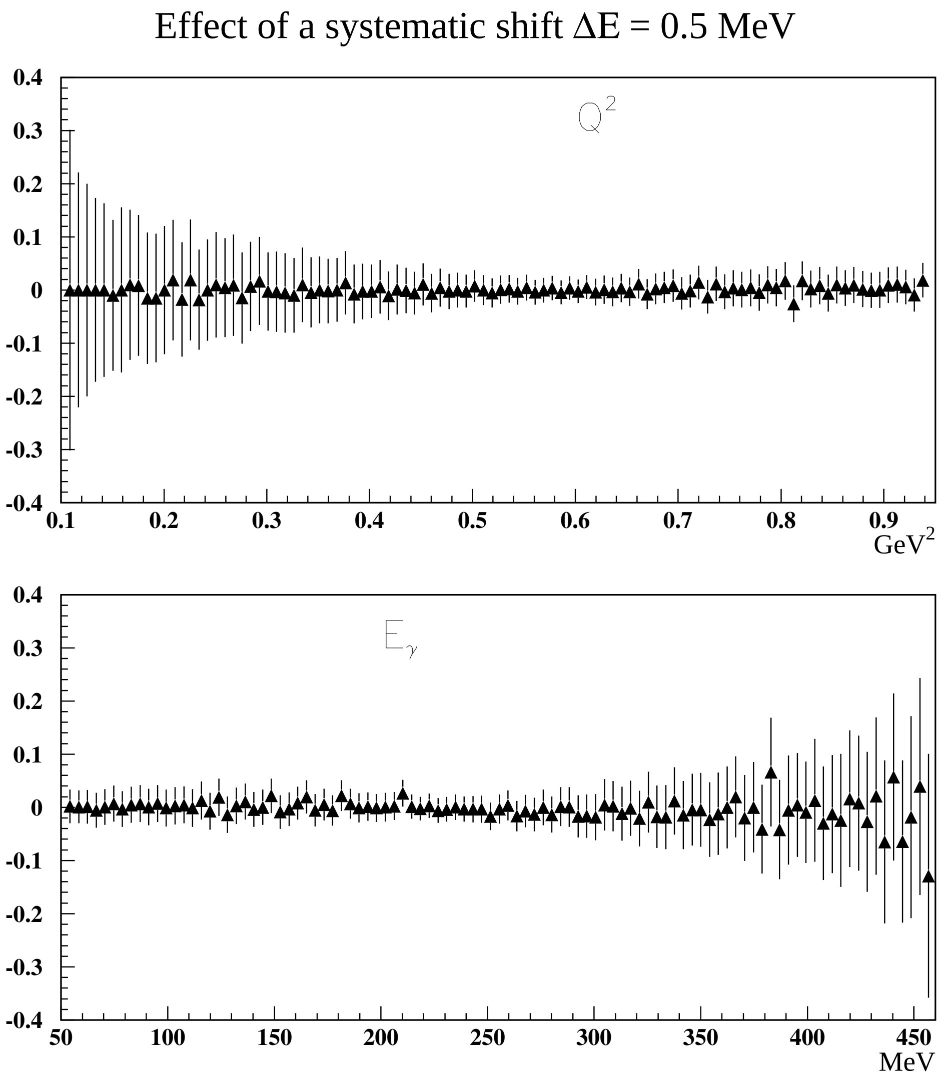

Figure 14: Effect of a systematic shift of 0.5 MeV on Q^2 (up) and E_γ (down) spectrum, assuming a partition of 100 bins. The difference in population due to the shift, normalized to the nominal one (no shift), is given for each bin of energy.

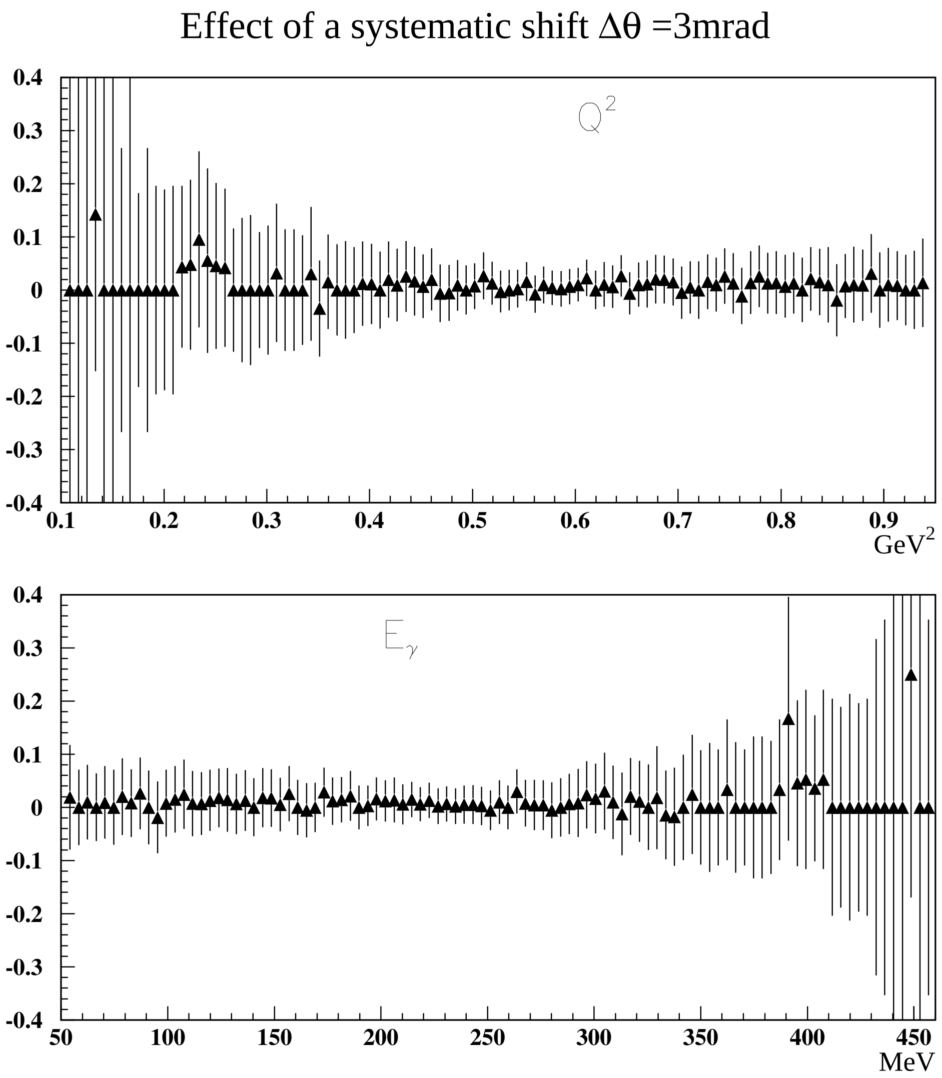

Figure 15: Effect of a systematic shift of 3 mrad on on Q^2 (up) and E_γ (down) spectrum, assuming a partition of 100 bins. The difference in population due to the shift, normalized to the nominal one (no shift), is given for each bin of energy.

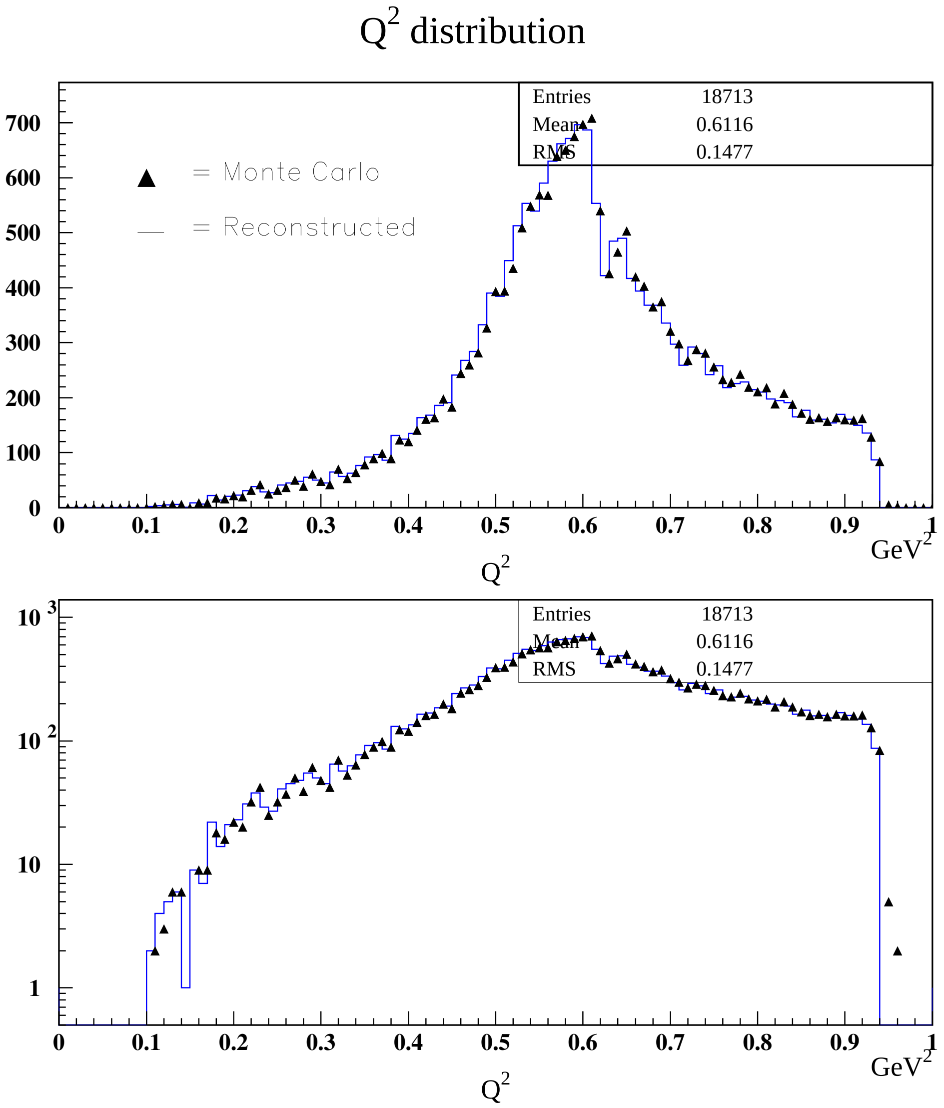

Figure 16: Comparison of the invariant mass distribution of the reconstructed pions with the expected Monte Carlo one, both in linear (up) and logarithmic scale(down).

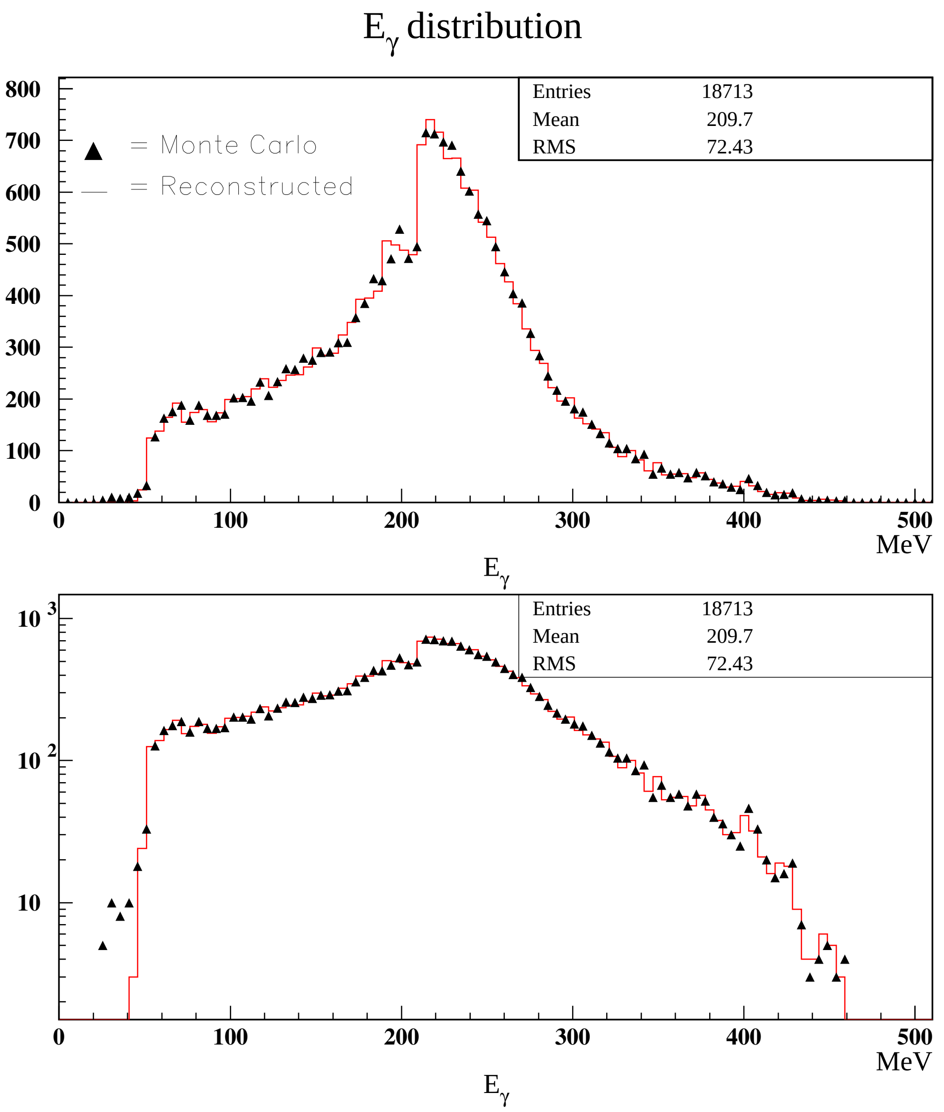

Figure 17: Comparison of the reconstructed energy of the extrapolated photon with the expected Monte Carlo one, both in linear (up) and logarithmic scale(down).

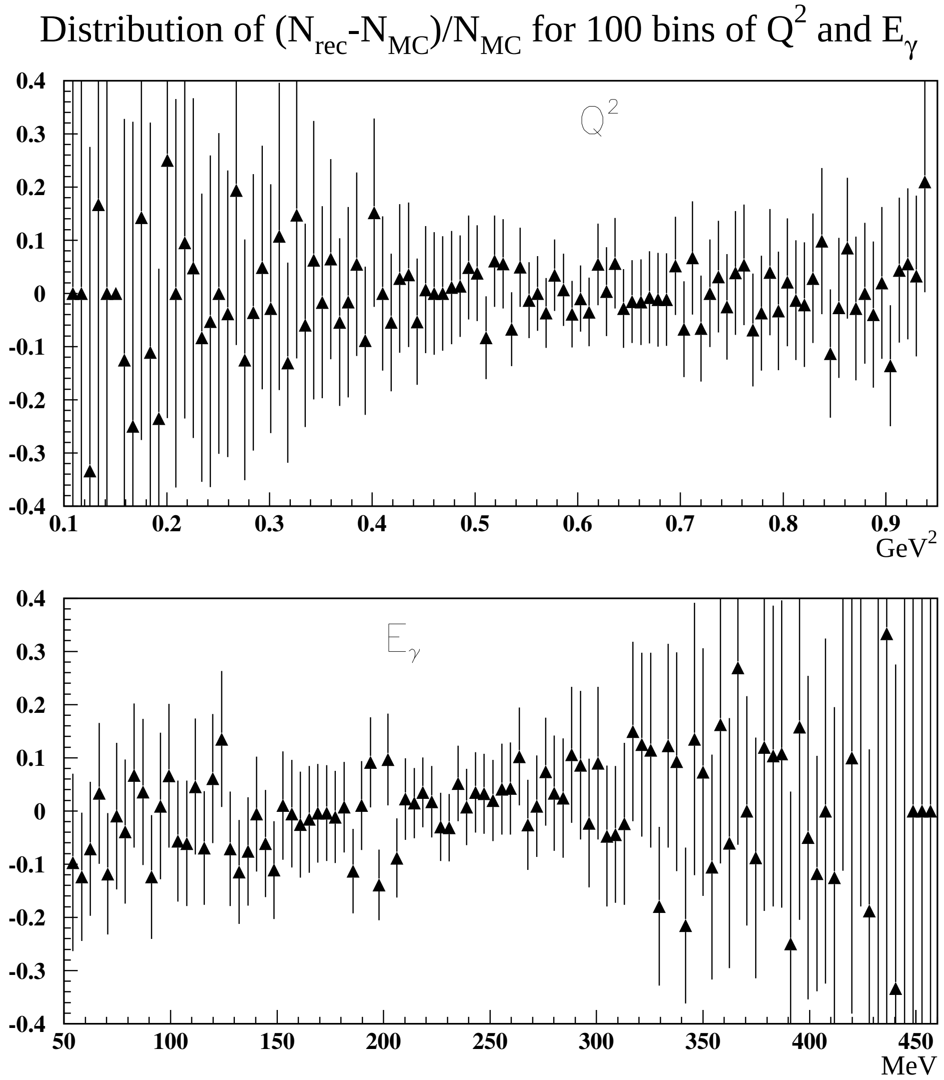

Figure 18: Effect of the detector resolution on Q^2 (up) and E_γ (down) spectrum, assuming a partition of 100 bins. The difference in population for reconstructed and Monte Carlo data, normalized to the Monte Carlo one, is given for each bin of energy.

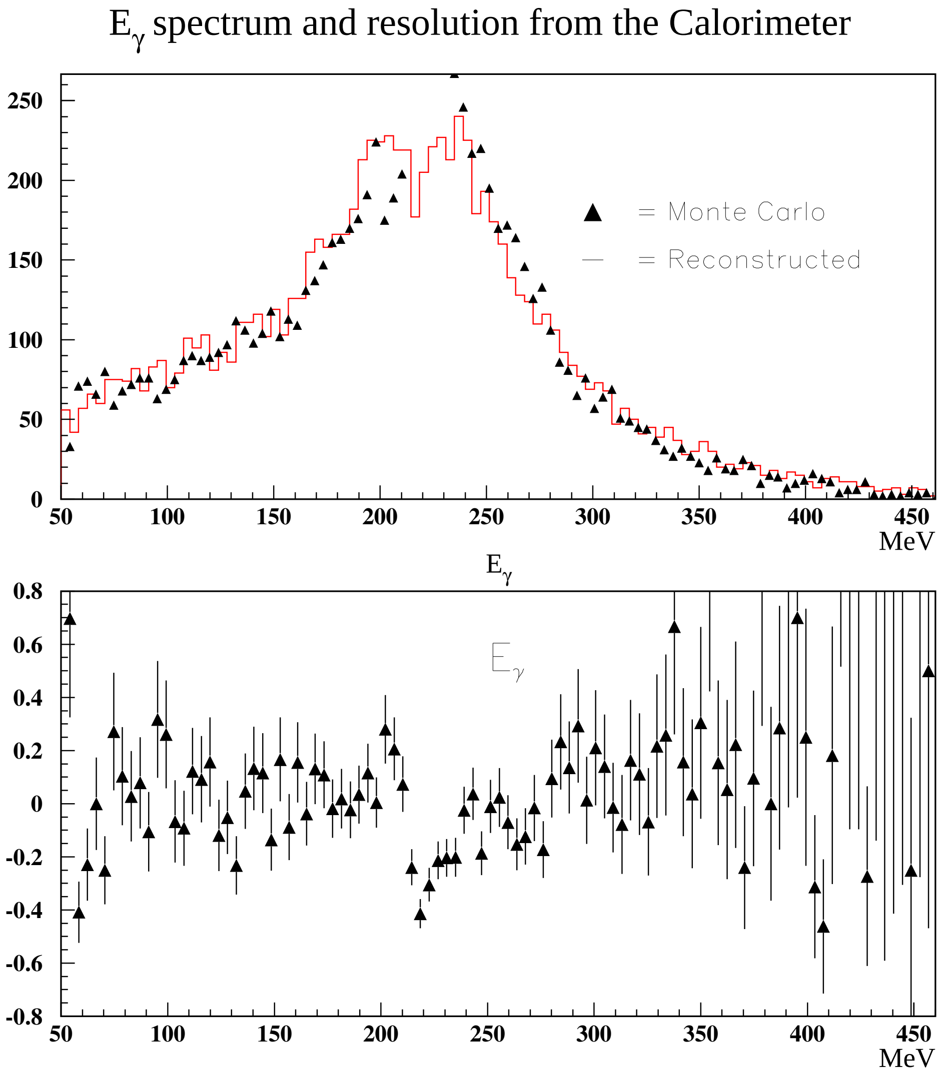

Figure 19: Resolution on the energy of the photon reconstructed with the Calorimeter. (Up) Comparison between the reconstructed and the Monte Carlo distributions; (down) Effect of the resolution on E_γ, assuming a partition of 100 bins. The difference in population for the reconstructed and Monte Carlo data, normalized to the Monte Carlo one, is given for each bin of energy. Note the different scale w.r.t. Fig. 18

6 Conclusion

A detailed Monte Carlo study of $e^+e^- \rightarrow \pi^+\pi^-\gamma$ with the initial state radiation for the measurement of the hadronic cross section $\sigma(e^+e^- \rightarrow \pi^+\pi^-)$ with the KLOE detector has been presented. The updated version of the KLOE reconstruction program has been applied. An identification procedure has been worked out which allows to obtain a hadronic cross section for $\pi^+\pi^-\gamma$ from *i.s.r.* of $3.7nb$ and a contamination from *f.s.r.* of the order of 1%. The effects arising from statistics, systematics, detector resolution and background rejection on the precise evaluation of $\sigma(e^+e^- \rightarrow \pi^+\pi^-)$ at the 1% level for each bin of energy have been discussed. No substantial limitations have been found to achieve such a challenging task. Some further extensions of our identification procedure have been discussed. Work is going on in order to produce a large statistics sample of events and to refine the Monte Carlo calculations.

Acknowledgements

We would like to thank J.H.Kühn and K.Melnikov for providing us their Monte Carlo generator and very useful discussions and critical remarks. We also benefited of discussions with F.Jegerlehner, V.Khoze and G.Pancheri.

This work is supported by the European Union Network EURODAPHNE, contract N^o $FMRX-CT98-0169$ and the German Ministry of Education and Technology BMBF, contract N^o $06-KA-860$.

References

[1] Detailed references on the measurement of hadronic cross sections at DAΦNE can be found in the proceedings of the Workshop on 'Hadron production cross sections at DAΦNE', Karlsruhe, Nov. 1 and 2, 1996, Ed. U.v.Hagel, W.Kluge, J.Kühn, G.Pancheri;

[2] S.Eidelman, F. Jegerlehner, Z. Phys. **C 67** (1995) 585-602;

F.Jegerlehner *Precision measurement of hadronic cross-sections at low energies* EURODAΦNE Meeting, LNF, Frascati, Italy (1998);

F.Jegerlehner *Hadronic effects in* $(g-2)_\mu$ *and* $\alpha_{QED}(M_Z)$*: Status and perspectives*, Preprint DESY99-007, hep-ph/9901386;

F.Jegerlehner *Sigma Hadronic and Precision Tests of the SM*, LNF Spring School and EURODAΦNECollaboration Meeting, Frascati, Italy (1999);

[3] N.Cabibbo, R.Gatto, Phys. Rev. **124** (1961) 1577;

[4] 1 P.Franzini, *The muon gyromagnetic ratio and R_h at DAΦNE*, The Second DAΦNEPhysics Handbook, INFN-LNF (1995), Ed.s L.Maiani, G.Pancheri, N.Paver, Vol.2, 471;

[5] E821 Collaboration (B.L. Roberts *et al.*) *The new muon (g-2) experiment*, in the proceedings of 28th International Conference on High-energy Physics (ICHEP'96), Warsaw, Poland, 25-31 July 1996.

[6] S.Spagnolo, "*La camera a drift di KLOE e prospettive e obiettivi di una nuova misura delle correzioni adroniche al g-2 del muone a DAΦNE*", Doctorate thesis (in Italian), University of Lecce, 1999, unpublished;

[7] S.Eidelman, F.Jegerlener, A.L.Kataev, O.Veretin, *Testing non-perturbative strong interaction effects via the Adler function*, preprint DESY 98-206, hep-ph/9812521;

[8] V.N.Baier, V.A.Khoze, Sov. Phys. JETP **21** (1965) 1145;

M.J.Creutz, M.B.Einhorn, Phys. Rev. **D 9** (1970) 2537;

A.B.Arbuzov, E.A.Kuraev, N.P.Merenkov and L.Trentadue, JHEP **12** (1998) 009;

S.Binner, J.H.Kühn and K. Melnikov, hep-ph/9902399;

M.Konchatnij, N.P.Merenkov, hep-ph/9903383;

[9] S.Spagnolo *The Hadronic Contribution to the Muon g-2 from Hadron Production in Initial State Radiation Events at the e^+e^- Collider DAΦNE* Eur.Phys.J **C6** 637-645(1999) and LNF-98/028(IR)

[10] S.Binner *et al* of ref. [8]

[11] C.Bini e P.Gauzzi, KLOE Memo No.171/98

[12] A. Bramon and M. Greco, *Scalar mesons and $\phi \to \pi^+\pi^-\gamma$ at DAΦNE*, The Second DAΦNEPhysics Handbook, INFN-LNF (1995), Ed.s L.Maiani, G.Pancheri, N.Paver, Vol.2, 663

[13] A.Farilla, W.Kim, J.Lee-Franzini, KLOE Memo No. 82/97 and KLOE Memo No. 123/97;

A.Farilla, S.Giovannella, J.Lee-Franzini, KLOE Memo No. 145/98;

[14] A.Denig, "*Aufbau, Automatisierung und Test eines Gassystem für die KLOE-Driftkammer und Untersuchungen zur Messung der Pionpaarerzeugung mit Photonabstrahlung bei DAΦNE*", Doctorate Thesis (in German), University of Karlsruhe, 1999, unpublished;

[15] G.Cabibbo G.Venanzoni, KLOE Memo NO. 168/98 and EuroDAΦNE internal Note 98-16;

[16] G. Montagna, presentation given to the workshop on the luminosity and hadronic cross section, LNF October 6 1998;